Article

Compressing High Energy Lasers through Optical Polymer Films

Jonathan Wheeler [1],[*],[†], Gabriel Petrişor Bleotu [2],[3],[4], Andrei Naziru [2],[4], Riccardo Fabbri [2], Masruri Masruri [2], Radu Secareanu [2], Deano M. Farinella [5], Gabriel Cojocaru [2],[6], Razvan Ungureanu [6], Elsa Baynard [7], Julien Demailly [7], Moana Pittman [7], Razvan Dabu [2], Ioan Dancus [2], Daniel Ursescu [2],[4], David Ros [7], Toshiki Tajima [5] and Gerard Mourou [1]

[1] DER-IZEST, Ecole Polytechnique, Route de Saclay, 91128 Palaiseau, France
[2] Extreme Light Infrastructure-Nuclear Physics, National Institute for R&D in Physics and Nuclear Engineering (IFIN-HH), 30 Reactorului, 077125 Magurele, Romania
[3] LULI-CNRS, CEA, Institut Polytechnique de Paris, Universite Sorbonne, Ecole Polytechnique, 91128 Palaiseau CEDEX, France
[4] Department of Physics, University of Bucharest, 077125 Magurele, Romania
[5] Department of Physics and Astronomy, University of California, Irvine, CA 92697, USA
[6] Center for Advanced Laser Technologies (CETAL), National Institute for Laser, Plasma and Radiation Physics (INFLPR), 409 Atomistilor, 077125 Magurele, Romania
[7] Laboratoire de Physique des 2 Infinis Irène Joliot-Curie—IJCLab, UMR9012—CNRS/Université Paris-Saclay/Université de Paris, 91405 Orsay CEDEX, France
[*] Correspondence: jonathan.wheeler@auspexphotonics.com
[†] Current address: Independent Researcher, 92340 Bourg-la-Reine, France.

Abstract: The thin-film post-compression technique has the ability to reduce the pulse duration in PW-class lasers, increasing the peak power. Here, the nonlinear response of an increasingly available optical thermoplastic demonstrates enhanced spectral broadening, with corresponding shorter pulse duration compared to fused silica glass. The thermoplastic can be used close to its damage threshold when refreshed using a roller mechanism, and the total amount of material can be varied by folding the film. As a proof-of-principle demonstration scalable to 10-PW, a roller mechanism capable of up to 6 passes through a sub-millimeter thermoplastic film is used in vacuum to produce two-fold post-compression of the pulse. The compact design makes it an ideal method to further boost ultrahigh laser pulse intensities with benefits to many areas, including driving high energy acceleration.

1. Introduction

High power laser facilities produce energies of tens to hundreds of Joules contained within pulse durations of tens of femtoseconds (10^{-15} s) thus reaching the class of Petawatt (PW: 10^{15} W). PW-class laser systems based on Chirped Pulse Amplification (CPA) [1] and Optical Parametric Chirped Pulse Amplification (OPCPA) [2] technologies are becoming more and more common all over the world. These laser facilities, such as LASERIX [3], HPLS at ELI-NP [4,5], CETAL-PW [6], Apollon [7,8], BELLA [9], CoReLS [10], SULF [11], etc. are operating at various repetition rates and reaching ever-increasing peak intensities. Such systems deliver laser pulses with duration in the range of 25 fs at a central wavelength of $\lambda_0 \sim 800$ nm, corresponding to ~ 10 optical cycles for the single-cycle period of $T_0 \sim 2.5$ fs.

Post-compressing these pulses while preserving their energy, economically increases the achievable peak intensity of the pulse for experiments that use extreme fields. In addition, reducing the number of optical cycles in the pulse helps in the elimination of cycle-averaging in the investigation of physical processes that occur at this timescale, such as X-ray generation [12–15] and ion acceleration [16,17]. Studies predict achieving high energy, single or few-cycle laser pulses leads to improved conversion efficiency in these

laser-driven processes, in addition to boosting the intensity. These gains open a path for ascending toward Exawatt (EW) class lasers with benefits for the next stage of high field scientific investigation of processes such as QED studies, as drivers for particle acceleration, in relativistic compression to attosecond pulses, and X-ray crystal wakefield accelerators [18,19].

The post-compression of TW scale (10^{12} W) table-top mJ laser systems with Gaussian beam profiles is already a mature technique applied in many laboratories around the world [20] relying on designs involving gas-filled, hollow-core capillaries [21,22], multiple plate post-compression [23], or multipass Harriott cells [24,25]. These current compression techniques prove difficult to apply to Joule-level lasers, primarily due to the high intensity creating unstable plasma effects within the nonlinear materials at the focus of the beam. However, during the beam transport in PW-class, short pulse laser systems, the beam propagates at sufficient intensities to drive nonlinear processes in the near field that modify the initial pulse spectrum if the pulse is transmitted through a material. If the material thickness is properly controlled across the flat-top mode of the large aperture beam of high energy laser systems, the nonlinear optical processes can lead to significant spectral broadening while avoiding significant degradation of the profile. Several methods of employing a thin nonlinear element for pulse compression have been suggested [26].

Here, the emphasis is placed on self-phase modulation (SPM) within a thin (sub-millimeter) film, where the broadening of the spectrum is proportional to the nonlinear response due to the time-dependent change in intensity. The subsequent broadened, but chirped, pulse spectrum requires correction of the second order phase, or Group Delay Dispersion (GDD), due to the SPM process as well as the material dispersion in order to attain the new transform limited pulse duration [27]. This is typically managed by balancing the number of reflections from negative-dispersion mirrors, often referred to as chirped mirrors, along with any subsequent transmission through optical materials contributing additional positive dispersion, as shown in Figure 1. This configuration is referred to as a Thin Film Compressor (TFC), or the Compression AFter Compressor Approach (CAFCA) [28–30]. The primary impact on pulse energy due to the TFC is incurred by reflection losses at the thin film surfaces, typically no more than 5%. Minimizing these losses implies an efficiency of the pulse compression process that permits implementation of one or more TFC assemblies to extend the capability of existing laser infrastructures toward their fundamental limit of a single optical cycle.

Studies of high energy pulse post-compression has considered the nonlinear interaction with thin wafers made of crystal [31], glass [32,33], or plastic [29,34]. To date, the most powerful implementations employ glass plates and have shown the capability of producing with 14 J, 22 fs pulses spectra supporting sub-10 fs [35], compression of a 3.24 J pulse from 24 to 13 fs [36], compression of a 17 J pulse from 70 to 17 fs [37], an 18 J pulse compressed from 64 to 11 fs [38], and compression to sub-10 fs of a 2.5 J, 23 fs pulse [39]. Despite the many demonstrations using glasses, these plates often show thickness variations due to the manufacture process that cannot be polished over large apertures. The implementation with polymers is expected to prove more economical in producing the uniformity over the large film areas required to accommodate the beam sizes (often ~0.5 m) of multi-PW laser systems.

In this paper, a novel plastic film, specifically cyclic olefin polymer (COP, brandname ZeonorFilm™) is first tested [40]. COP is used in the economical production of optical components such as lenses, but its nonlinear response is not widely reported.
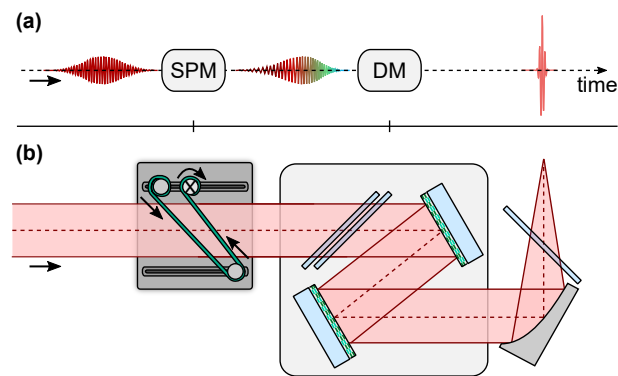
(a)

(b)

Figure 1. The conceptual steps from initial to post-compressed pulse of the TFC technique are shown in (**a**) that correspond to the laboratory configuration in (**b**). Relying on the uniform intensity profile of the beam, the femtosecond pulse passes through enough thin film material to induce sufficient SPM. The resultant chirped pulse achieves the optimized duration by the dispersion management (DM), which includes fixed negative GDD elements (i.e., chirped mirrors) balanced with the GDD of any additional optical elements (e.g., thin plates, turning mirrors, off-axis paraboloid or debris shield).

New classes of thin, high-quality optical films are becoming available on the market, intended primarily for new screen technologies in the electronics industry. The index of refraction n for COP is 1.53; its *GDD* value is 70.219 fs^2/mm at 800 nm. COP is known to be resistant to changes in its birefringence under stress; this offers an ideal alternative to plastic materials such as PMMA whose birefringence is known to vary with tension. This type of optical film is chosen also because it can be attained in rolls of a format ($100(l) \times 1(w)$ m^2 of 100–180 μm thick films) that economically accommodates the large beam sizes of 0.5 m diameter expected for 10 PW laser systems. The rolls can be sliced to appropriate widths for the beam diameter during the manufacturing process. The principle is to employ a roller mechanism which allows continual replacement of the material if it should degrade. Such a design is shown in Figure 1 where the thin film is held in a roller assembly that folds the long film to pass several times in the beam, so that the beam transits sufficient material for the desired spectral modification. By using a series of 100 μm thick films rather than a single bulk substrate, the amount of material interacting with the pulse can be optimized to the minimal required at the given initial pulse intensity and minimizes contributions to the B-integral and dispersion from excess material.

In this paper, the nonlinear properties of thin COP sample are measured to compare its effectiveness as an SPM material relative to typical fused silica wafers. A small-scale prototype of a Film Roller Mechanism (FRM) has been built, and experimental results using the TFC technique and the FRM within a vacuum environment are presented from measurements performed at the LASERIX laser platform [41] using a COP sample, and a 45 fs pulse with variable energy up to 500 mJ within an 18 mm diameter beam. The resulting pulse duration reduction is compared to simulations. Because the FRM prototype design is intended to be scaled to multi-centimeter beam sizes typical at Petawatt laser facilities, the requirements for TFC to be performed at the multi-PW level are presented based on the measured nonlinear properties of COP.

2. Experiment Setup

Figure 2 shows perspective views of the FRM, panel (a), and the layout of the configuration used in the experiment, panel (b).

The pulse interacts with the target film within a vacuum chamber immediately following the laser compressor. A variable attenuator (VA) consisting of a waveplate/polarizer combination is placed before the compressor in order to vary the energy of the pulse incident on the thin film. The FRM holding the COP film is placed in the experimental vacuum chamber immediately after the compressor. After interacting with the film, the pulse is attenuated by partial reflection (PR1) from two uncoated fused silica mirror substrates for

an expected reflectivity of 8% each. This attenuation prevents further SPM or damage to subsequent optics during the propagation of the pulse to the diagnostics bench, outside the vacuum chamber. The vacuum window is 5.1 mm thick and made of MgF_2 to minimize the additional dispersion introduced by traversing this optical component path to +100 fs^2. A beam-splitter (PR2) transmits 2% of the beam energy towards a lens of focal length f = 300 mm used for the imaging diagnostics (IM box) of the near and far fields (NF and FF, respectively) thus allowing for qualitative monitoring of the collimated and focused beam mode profiles. PR2 has a reflectivity of 98%, so that 0.6% of the original interaction energy is directed through the dispersion management (DM box) toward the pulse diagnostics (DG box). The DM begins with an adjustable aperture that reduces the beam diameter to the input size of the pulse diagnostics ($\leq$5 mm), and permits, by a slight variation in the angle of incidence on the first mirror, to vary the number of passes through a pair of chirped mirrors to provide 2, 4, or 6 bounces (typically 4 bounces). The chirped mirrors (CM; Ultrafast Innovations, HD58) provide a GDD of -250 fs^2 per bounce. As the CM overcompensate the initial pulse chirp, combinations of glass windows (W) made of fused silica or magnesium fluoride are inserted within the beam for control of the final measured pulse duration. Two temporal diagnostics (Light Conversion TIPA Single-shot Autocorrelator—AC; FastLite WIZZLER—WZ) record the pulse duration in parallel in order to verify the accuracy of the measurement. The WIZZLER is capable of retrieving the spectral phase of the pulse, which allows for the optimization in the final pulse compression. A fiber spectrometer (SP; Ocean Optics USB2000) also records the spectrum of the pulse for comparison with that recovered from the other diagnostics.
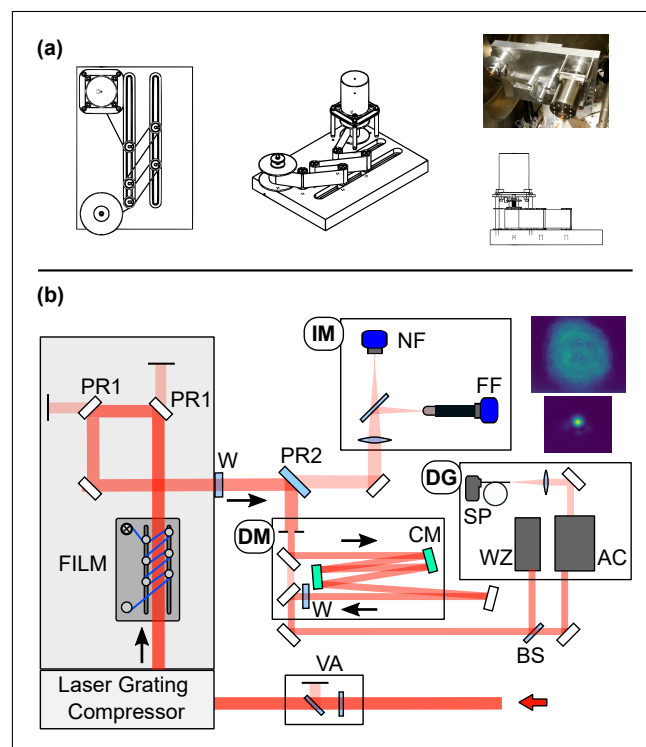

Figure 2. Perspective views and in situ photograph of the FRM prototype are shown in (**a**). The layout of the experiment as described in the text is pictured in (**b**).

In addition to the investigation performed with 0.1 mm thick COP film in the roller mechanism, measurements with a single fused silica window (University Wafers) of 0.5 mm thickness and 50 mm diameter act as a reference measurement for comparison to a material with known value of the nonlinear component of the refractive index n_2. The fused silica plate is mounted under vacuum at the same location as the FRM prototype, with sufficient translation for the samples to be moved in and out of the beam path without breaking

vacuum. The COP films are mounted near to Brewster's angle with respect to the incoming beam, resulting in an effective thickness of 0.69 mm for a 6-pass configuration.

3. Results

3.1. Nonlinear Material Response

The nonlinear intensity-dependence of the refraction index of materials $n(t) = n_o + n_2 \cdot I(\mathbf{x}, t)$ depends on the time-dependent pulse intensity I and gives rise to SPM as it propagates over an interaction length Δz within a material due to the rapid change in the pulse intensity over the pulse duration. In the case of a flat-top beam profile, where the spatial variation in the pulse intensity is minimized, the induced spectral shift $\delta\omega_{rel}$ relative to the fundamental frequency ω_o is expected to be uniform across the pulse profile and is derived from the definition of the instantaneous angular frequency, $\omega(t) = \omega_o + \delta\omega_{rel}(t)$. The spectral shift is thus expected to be proportional to $\frac{\partial I}{\partial t}$ by the definition of $\omega(t) = \frac{d\phi}{dt}$, where $\phi = \omega_o t - kz$ for the wave vector $k = k_o\, n(t)$, or

$$\delta\omega_{rel}(t) = \omega(t) - \omega_0 = \frac{d\phi}{dt} - \omega_0 = k_0 n_2 \frac{dI(t)}{dt}\Delta z . \tag{1}$$

As the intensity of the pulse retains a Gaussian temporal envelope, the time variation of the pulse intensity profile is expected to vary as $\frac{dI(t)}{dt} \sim I_o/\tau_p$, where the peak intensity is estimated by the input pulse energy E_p, pulse duration τ_p and the effective area of the pulse A_p by the relation $I_o \propto E_p/(\tau_p \cdot A_p)$ [42]. An estimate to the extent of the bandwidth after spectral broadening can then be estimated from Equation (1) in terms of readily measured beam quantities,

$$\delta\omega_{rel} = k_0 n_2 z \left.\frac{dI(t)}{dt}\right|_{max} \propto \frac{k_0 n_2}{\tau_p^2 A_p}(E_p \cdot \Delta z) . \tag{2}$$

The COP response is investigated, keeping the amount of film constant at six passes and varying the pulse energy in order to see the response to the changing laser intensity. For each energy value, several shots (from five to ten) are performed. The pulse spectral amplitude (red) and phase (green) as measured with the WIZZLER are presented in Figure 3a as a function of the input energy. When available, the reference spectrum is superimposed in gray color. The latter was measured with the FRM removed from the beam line; only two energy points ($E_p = 78.7$ mJ and $E_p = 157.9$ mJ) are available, with pulse energy values similar to the ones used with COP films. The phases for the reference spectra are flat as the compressor was adjusted during the experiment to deliver the optimized pulse duration.

The curves correspond to the mean values of the respective laser shots. The shaded band indicates the uncertainty estimated as half of the maximum deviation between the measurements.

The pulse bandwidth and duration values are given in Table 1 as function of the input energy E_p. For each shot measurement, the pulse bandwidth is calculated as the RMS of spectrum $\Delta\nu_\sigma$. For each energy point, the mean value is then calculated, and its uncertainty estimated as half of the maximum deviation. A Gaussian fit is superimposed on the reconstructed pulse duration, and the extracted FWHM along with its fit uncertainty is used to estimate the pulse duration τ_p. The pulse parameters are also presented as a function of the scaling variable $\xi \equiv E_p \cdot \Delta z$, Δz being the target thickness in millimeters. The expected increase (decrease) is seen in the trend for the bandwidth (pulse duration) as a function of increasing input pulse energy with a fixed amount of material.
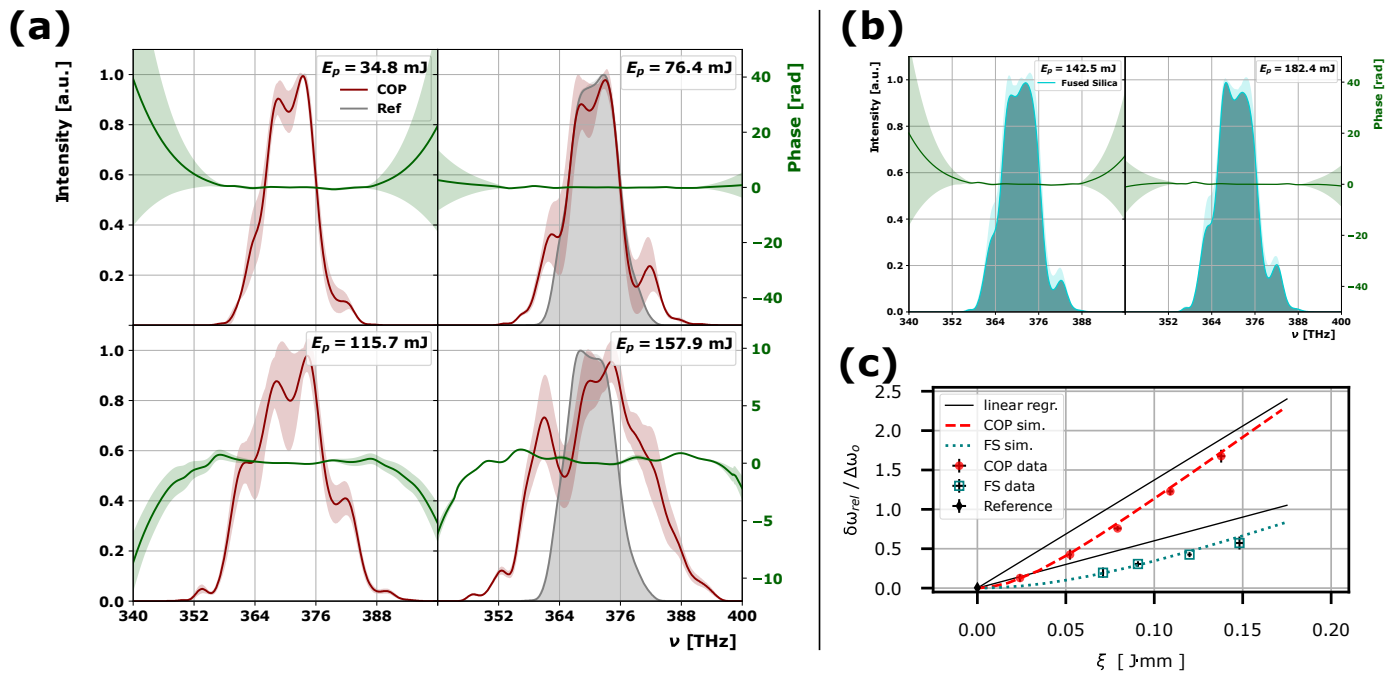
(a)

(b)

(c)

Figure 3. The measured spectra and phase response of the pulse passing through six layers of COP film are shown in (**a**). The pulse energy increases from top left to bottom right, corresponding to 35 mJ, 76 mJ, 116 mJ and 158 mJ, respectively. Superimposed in gray are the original spectra measured with no material present. In (**b**), the spectra and phase measured using a fused silica (FS) plate are shown. The measured response of the COP film is compared with FS in (**c**). The induced bandwidth ($\delta\omega_{rel}$) relative to the original reference bandwidth $\Delta\omega_o$ of the input pulse is shown vs. the parameter ξ. A linear regression performed on the two data-sets is superimposed on the measurements (solid line), as well as the results obtained from simulations (dashed lines).

Table 1. Measured pulse parameters for reference pulse with no film installed (NA), 6× COP with total effective thickness of 0.69 mm, and fused silica (FS) wafers.

Film	E_p [mJ]	ξ [J·mm]	$\Delta\nu_\sigma$ [±0.4, THz]	$\Delta\lambda_{FWHM}$ [±2, nm]	τ_p [fs]
NA	all	–	4.1	21	45.5
COP	35	0.025	4.6	24	43.3
COP	76	0.054	5.9	30	32.6
COP	116	0.081	7.2	37	29.4
COP	158	0.112	9.2	47	23.4
FS	143	0.071	4.9	25	39.8
FS	182	0.091	5.4	28	36.3
FS	240	0.120	5.9	30	31.9
FS	296	0.148	6.4	33	29.0

The resulting pulse duration of 23 fs is half the original pulse duration of 45 fs in the highest energy case, with little adverse modification in the beam.

In order to better simulate the SPM response for the COP material, it is necessary to extract the nonlinear response n_2 of the material from the data, as there is limited information provided for this material within the femtosecond regime around 800 nm in the literature at this time. In considering the extent of the bandwidth shift after spectral broadening ($\delta\omega_{rel}$), Equation (2) gives the expected response. The majority of these parameters ($f(k_o, \tau_p, A_p)$) depend on the laser conditions and remain constant throughout the experiment, except for the varied input pulse energy E_p and the interaction distance Δz due to the thickness

of the material. This simplifies the multivariate dependence on spectral broadening of Equation (1) by studying the spectral broadening as a function of the variable $\xi = E_p \cdot \Delta z$,

$$\delta\omega_{rel} \propto \frac{k_0}{\tau_p^2 A_p} \cdot n_2 \cdot (E_p \cdot z) \equiv C_L \cdot n_2 \cdot \xi. \tag{3}$$

From the simplified Equation (3), a linear dependence of the shift of the frequency relative to ξ is expected from the assumed approximation. The slope can be separated into two factors, the material-dependant n_2 and the constant factor C_L that depends on the laser pulse geometry, $m = C_L \cdot n_2$. This demonstrates that the spectral broadening measured for a specific material should fit a straight line with respect to the variable ξ. The slope m of the linear regression to the data is thus proportional to the n_2 for a given material. The unknown parameter n_2 of COP can be then estimated by comparing the extracted fit slope m of COP response to that of the well known material Fused Silica (FS), $m_{COP}/m_{FS} = n_2^{COP}/n_2^{FS}$. The spectrum and phase were thus measured using a single 0.5 mm thick fused silica plate at normal incidence; two example spectra are shown in Figure 3b for different values of pulse energy, and the measured parameters are also presented in Table 1.

The relative maximum spectral shift due to SPM ($\delta\omega_{rel}$) is approximated from the experiment by subtracting the initial reference bandwidth ($\Delta\omega_o$) from the bandwidth measured after SPM ($\Delta\omega_{spm}$): $\delta\omega_{rel} \sim \Delta\omega_{spm} - \Delta\omega_o$. The comparison of measured relative spectral shift for six passes of COP at a thickness of 0.1 mm (6× COP) with a Fused Silica plate at normal incidence is presented in Figure 3c. The response of the COP film is significantly larger than the fused silica. A linear regression is performed on the two data-sets and superimposed to the measurements as black lines in Figure 3c. The ratio of the slopes extracted from the linear fits of the COP to fused silica data ($m_{COP}/m_{FS} = 2.3 \pm 0.1$) gives access to n_2^{COP} using the known value for fused silica, $n_2^{FS} = 2.4 \times 10^{-4}$ cm^2/TW. [43] Therefore, the value n_2 for COP at 800 nm can be estimated to be $n_2^{COP} = (2.3 \pm 0.2)\, n_2^{FS}$,

$$n_2^{COP} = (5.5 \pm 0.6) \times 10^{-20} \text{ m}^2/\text{W}.$$

The simplified estimate used for the relative spectral broadening is a linear function of ξ and is shown in Figure 3c by the solid black lines with the extracted slope to not fit the data well. The estimated value of n_2^{COP} is then used in the simulations based on the Python nonlinear optics package pyNLO [44], and overlaid on the experimental data in Figure 3c as dashed lines. The simulation is able to better demonstrate the observed behavior by using the respective values for n_2 and taking into account the reflection loss at each surface due to the angle of incidence (θ_i) with each film. The transmission for a surface is calculated using the typical Fresnel equations for p-polarized light $\left(T(\theta_i) = 1 - R_p(\theta_i)\right)$. The first five COP films were measured with $\theta_i = 50^o$ (T = 0.99/surface) while due to space constraints the final film was reduced so that $\theta_i = 23^o$ (T = 0.93/surface). The entire stack of six films should then result in a total transmission, $T_{tot} = (0.99)^{10} \times (0.93)^2 = 0.78$. In general, each film has a total transmission of 98% and if the final film had been at a similar θ_i then the $T_{tot} = (0.99)^{12} = 0.89$ for the series of six films. For the single FS film at normal incidence, the $T_{tot} = 0.96$.

3.2. Beam Profile

With the camera monitoring the near-field to detect damage in the thin film, the ability to characterize the development of the multi-filamentation process due to modulation instabilities (MI) in the beam must be considered. In the modulation instability gain theory based on steady-state waves, the characteristic size, d, should rise exponentially during propagation until reaching the exit of the material, or the laser-induced damage threshold (LIDT) of the material. When the peak power of the pulse exceeds the critical power $P_{cr} = 3.79\lambda_0^2/(8\pi n_0 n_2)$ (~1.2 MW for COP at 810 nm), intense pulses with super-gaussian modes are susceptible to multi-filamentation through the modulation instability initiated by noise in the beam profile [45,46]. The characteristic size for maximum MI gain is given

by the parameter $d \approx \left(\frac{2\pi P_{cr}}{I_o} \right)^{1/2}$ which in the case of COP at $I_o \approx 1.4 \times 10^{12}$ W/cm^2 gives an approximate feature size of $d \approx 23$ μm [47], which is smaller than the near-field system is capable of resolving (46 μm with two pixels). The profile imaging will need to be further developed to better capture the crucial feature sizes relative to the earliest stages of damage. In Figure 4a, the discrete change in material with additional passes of the film ranges from a reference with no film, a single 0.1 mm thick film, 4× 0.1 mm thick films, and 6× 0.1 mm thick films are compared showing the increasing development in the modulation noise with increasing material interaction. If the beam modulations reached the point that material damage or discoloration occurred, it appeared in the final pass of the film so that partial shifts of the material are sufficient to refresh the film. Improved optimization in the number of passes, i.e., five, could also maximize the spectral broadening while minimizing any degradation in the spatial mode.
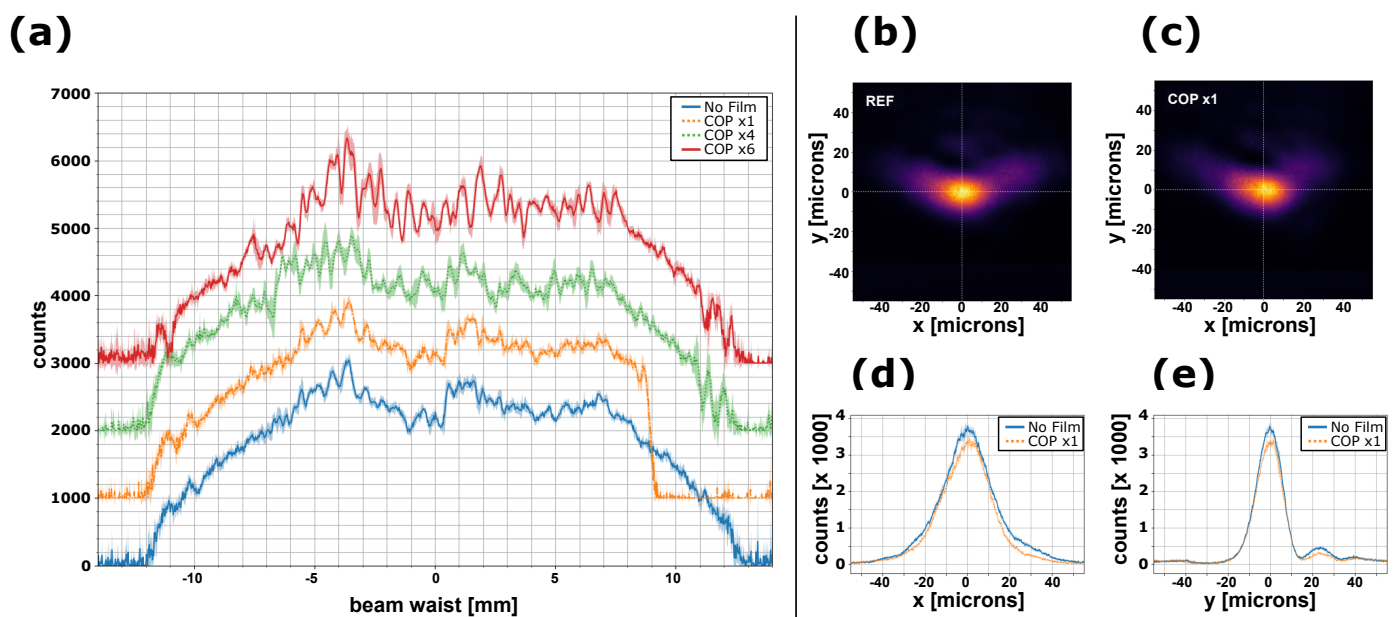

Figure 4. Beam profile with COP film. In (**a**) central line outs from near field images are compared with increasing number of film passes from bottom to top: reference beam (no film); a single 0.1 mm film (showing hard cut in beam due to mounting); 4× 0.1 mm; and 6× 0.1 mm, respectively. The input energy is kept at 160 mJ. In (**b**) the REF focus is shown without a film in place while (**c**) shows the focus after the 1× COP [0.1 mm] film is placed in the beam. In (**d**), the comparison with/ without the film in place of the horizontal line out is shown while (**e**) compares the same along the vertical axis.

Because the multipass spectral study was performed with a lower optical quality grade of COP, the focus from the single high quality COP film is also considered in order to demonstrate the effect on the beam's focusability. Typical focus images with no film (Ref) and with a single film (COP ×1) are shown in (b) and (c) of Figure 4, respectively. The line outs comparing the horizontal and vertical directions are given in (d) and (e) of Figure 4. The focus is not optimized even before the film is introduced, but there is no significant change in the structure of the focus with the inclusion of the film. The details of the profiles should be clarified by further studies implementing a deformable mirror for an improved initial focus, higher quality optical films, and an intentional imaging assembly for spatial characterization of the beam with better resolution.

4. Discussion

The results of these studies, measuring the compression from 45 fs down to 23 fs at a pulse fluence similar to the PW lasers at ELI-NP, point to achieving compression by at least

a factor of two for high peak power pulses containing Joules of energy. This will extend the capabilities of this new generation of high energy laser technology by compressing the current pulses of 25 fs by a similar factor [48]. The scalability of the COP film up to an aperture of 1 m makes this material suitable for implementation at normal incidence, or even Brewster's angle, for the large beam apertures of 10 PW-class systems, e.g., the 55 cm beam diameter at the HPLS 10 PW output. The simulations of the resulting increase in bandwidth for a 25 fs pulse at appropriate fluences for the 10 PW HPLS laser facility of ELI-NP are presented in Figure 5. As the pulse begins at 25 fs rather than the 45 fs of these experiments at LASERIX, less material is required. The simulation indicates that passing once or twice through films of thickness of 0.10 mm or 0.18 mm (labelled in the figure as COP 0.10 mm, COP 0.18 mm, COP 2× 0.10 mm, COP 2× 0.18 mm, respectively) is expected to achieve a significant spectral broadening, even enough to support a sub-10 fs pulse.
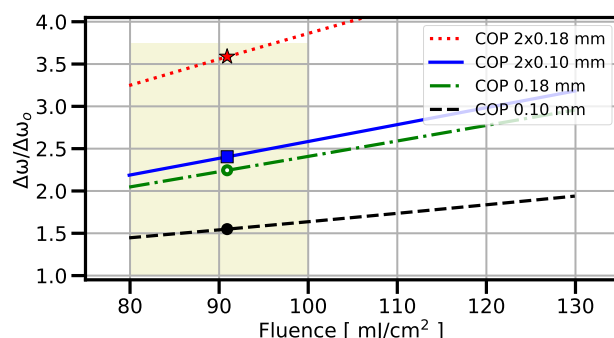

Figure 5. Simulated response of the COP film obtained from a 1-D simulation in PyNLO for initial pulse duration of 25 fs. The induced increase in bandwidth ($\Delta\omega$) relative to the original reference bandwidth $\Delta\omega_0$ of the input pulse is shown relative to pulse fluence for examples of a single film and two films. The shaded region highlights the values that correspond to the relevant pulse fluences of 80–100 mJ/cm^2. The points correspond to bandwidths supporting ftl pulse durations of 17.75 (●), 12.75 (○), 12.0 (■), 8.25 (★) fs.

As an example of an optimized design for a COP compressor, a pulse of 25 fs interacting with two passes of a 0.18 mm thick film of COP at Brewster's angle produces a bandwidth that supports a pulse of duration below 9 fs with a small compensation of only -70 fs^2 in GDD. This value reduces the challenges for the chirped mirror production, and also suggests the possibility to replace them with more conventional broadband mirrors with negative residual GDD. Another possibility is to use a second thin plate with thickness on the order of the wavelength in reflection [48]. Because the design consists of only two passes, the total transmission is expected to be $T_{tot} = (0.99)^4 = 0.96$. Such implementations would enable pulses with peak power in excess of 20 PW.

5. Conclusions

Optical-grade extruded thermoplastic films, such as COP, demonstrate great promise for nonlinear manipulation of high energy beams of large diameter aperture. The polymer shows greater uniformity in thickness for the cost than many glasses, or other rigid materials, at these dimensions. In addition, the larger n_2 value of the COP film concentrates the nonlinear B-integral contribution to the film rather than any additional elements made of glasses, e.g., debris shield, or thin plates for fine tuning the GDD with positive dispersion. Rolls of the film can be mounted using an FRM device for long-term use in the case when eventual degradation requires the material to be refreshed. An up-scaled version of the set-up can be demonstrated with existing technology and, in combination with adequate, less constrained dispersion management, it can provide practical access to pulses with peak power in excess of 20 PW. This is an efficient alternative, alongside the nonlinear amplification [49] and coherent combination methods, to generate Exawatt class lasers. The

compact design makes it an ideal method to further boost ultrahigh laser pulse intensities for driving high energy acceleration.

References

1. Strickland, D.; Mourou, G. Compression of amplified chirped optical pulses. *Opt. Commun.* **1985**, *56*, 219–221. [CrossRef]
2. Dubietis, A.; Jonušauskas, G.; Piskarskas, A. Powerful femtosecond pulse generation by chirped and stretched pulse parametric amplification in BBO crystal. *Opt. Commun.* **1992**, *88*, 437–440. [CrossRef]
3. Ple, F.; Pittman, M.; Jamelot, G.; Chambaret, J.P. Design and demonstration of a high-energy booster amplifier for a high-repetition rate petawatt class laser system. *Opt. Lett.* **2007**, *32*, 238. [CrossRef]
4. Lureau, F.; Matras, G.; Chalus, O.; Derycke, C.; Morbieu, T.; Radier, C.; Casagrande, O.; Laux, S.; Ricaud, S.; Rey, G.; et al. High-energy hybrid femtosecond laser system demonstrating 2 ∗ 10 PW capability. *High Power Laser Sci. Eng.* **2020**, *8*, e43. [CrossRef]
5. Gales, S.; Tanaka, K.A.; Balabanski, D.L.; Negoita, F.; Stutman, D.; Tesileanu, O.; Ur, C.A.; Ursescu, D.; Andrei, I.; Ataman, S.; et al. The extreme light infrastructure—Nuclear physics (ELI-NP) facility: New horizons in physics with 10 PW ultra-intense lasers and 20 MeV brilliant gamma beams. *Rep. Prog. Phys.* **2018**, *81*, 094301. [CrossRef]
6. Matras, G.; Lureau, F.; Laux, S.; Casagrande, O.; Radier, C.; Chalus, O.; Caradec, F.; Boudjemaa, L.; Simon-Boisson, C.; Dabu, R.; et al. First sub-25fs PetaWatt laser system. In Proceedings of the CLEO: 2013, San Jose, CA, USA, 11–13 June 2013; Paper CTh5C.5; OSA: Washington, DC, USA, 2013. [CrossRef]
7. Zou, J.; Le Blanc, C.; Papadopoulos, D.; Chériaux, G.; Georges, P.; Mennerat, G.; Druon, F.; Lecherbourg, L.; Pellegrina, A.; Ramirez, P.; et al. Design and current progress of the Apollon 10 PW project. *High Power Laser Sci. Eng.* **2015**, *3*, e2. [CrossRef]
8. Le Garrec, B.; Papadopoulos, D.N.; Le Blanc, C.; Zou, J.P.; Chériaux, G.; Georges, P.; Druon, F.; Martin, L.; Fréneaux, L.; Beluze, A.; et al. Design update and recent results of the Apollon 10 PW facility. In Proceedings of the SPIE 10238, High-Power, High-Energy, and High-Intensity Laser Technology III, Prague, Czech Republic, 26–27 April 2017; Hein, J., Ed.; International Society for Optics and Photonics: Bellingham, WA, USA, 2017; Volume 10238. [CrossRef]
9. Nakamura, K.; Mao, H.S.; Gonsalves, A.J.; Vincenti, H.; Mittelberger, D.E.; Daniels, J.; Magana, A.; Toth, C.; Leemans, W.P. Diagnostics, Control and Performance Parameters for the BELLA High Repetition Rate Petawatt Class Laser. *IEEE J. Quantum Electron.* **2017**, *53*, 1–21. [CrossRef]
10. Yoon, J.W.; Kim, Y.G.; Choi, I.W.; Sung, J.H.; Lee, H.W.; Lee, S.K.; Nam, C.H. Realization of laser intensity over 10^{23} W/cm^2. *Optica* **2021**, *8*, 630. [CrossRef]
11. Cartlidge, E. The light fantastic. *Science* **2018**, *359*, 382–385. [CrossRef] [PubMed]
12. Naumova, N.M.; Nees, J.A.; Sokolov, I.V.; Hou, B.; Mourou, G.A. Relativistic Generation of Isolated Attosecond Pulses in a λ^3 Focal Volume. *Phys. Rev. Lett.* **2004**, *92*, 063902. [CrossRef]
13. Naumova, N.M.; Nees, J.A.; Mourou, G.A. Relativistic attosecond physics. *Phys. Plasmas* **2005**, *12*, 056707. [CrossRef]

14. Ma, G.; Dallari, W.; Borot, A.; Krausz, F.; Yu, W.; Tsakiris, G.D.; Veisz, L. Intense isolated attosecond pulse generation from relativistic laser plasmas using few-cycle laser pulses. *Phys. Plasmas* **2015**, *22*, 033105. [CrossRef]

15. Zhang, Y.X.; Qiao, B.; Xu, X.R.; Chang, H.X.; Yu, M.Y.; Zhong, C.L.; Zhou, C.T.; Zhu, S.P.; He, X.T. Intense single attosecond pulse generation from near-critical-density plasmas irradiated by a few-cycle laser pulse. *Phys. Plasmas* **2018**, *25*, 023302. [CrossRef]

16. Zhou, M.L.; Yan, X.Q.; Mourou, G.; Wheeler, J.A.; Bin, J.H.; Schreiber, J.; Tajima, T. Proton acceleration by single-cycle laser pulses offers a novel monoenergetic and stable operating regime. *Phys. Plasmas* **2016**, *23*, 043112. [CrossRef]

17. Wu, X.Z.; Gong, Z.; Shou, Y.R.; Tang, Y.H.; Yu, J.Q.; Mourou, G.; Yan, X.Q. Efficiency enhancement of ion acceleration from thin target irradiated by multi-PW few-cycle laser pulses. *Phys. Plasmas* **2021**, *28*, 023102. doi: 10.1063/5.0029171. [CrossRef]

18. Wheeler, J.A.; Mourou, G.; Tajima, T. Science of High Energy, Single-Cycled Lasers. *Rev. Accel. Sci. Technol.* **2019**, *10*, 227–244. [CrossRef]

19. Tajima, T. Laser acceleration in novel media. *Eur. Phys. J. Spec. Top.* **2014**, *223*, 1037–1044. [CrossRef]

20. Mével, E.; Tcherbakoff, O.; Salin, F.; Constant, E. Extracavity compression technique for high-energy femtosecond pulses. *J. Opt. Soc. Am. B* **2003**, *20*, 105. [CrossRef]

21. Brabec, T.; Krausz, F. Intense few-cycle laser fields: Frontiers of nonlinear optics. *Rev. Mod. Phys.* **2000**, *72*, 545–591. [CrossRef]

22. Goulielmakis, E.; Schultze, M.; Hofstetter, M.; Yakovlev, V.S.; Gagnon, J.; Uiberacker, M.; Aquila, A.L.; Gullikson, E.M.; Attwood, D.T.; Kienberger, R.; et al. Single-cycle nonlinear optics. *Science* **2008**, *320*, 1614–1617. [CrossRef] [PubMed]

23. Cheng, Y.C.; Lu, C.H.; Lin, Y.Y.; Kung, A.H. Supercontinuum generation in a multi-plate medium. *Opt. Express* **2016**, *24*, 7224. [CrossRef] [PubMed]

24. Ueffing, M.; Reiger, S.; Kaumanns, M.; Pervak, V.; Trubetskov, M.; Nubbemeyer, T.; Krausz, F. Nonlinear pulse compression in a gas-filled multipass cell. *Opt. Lett.* **2018**, *43*, 2070. [CrossRef]

25. Lavenu, L.; Natile, M.; Guichard, F.; Zaouter, Y.; Delen, X.; Hanna, M.; Mottay, E.; Georges, P. Nonlinear pulse compression based on a gas-filled multipass cell. *Opt. Lett.* **2018**, *43*, 2252. [CrossRef]

26. Mironov, S.Y.; Wheeler, J.; Gonin, R.; Cojocaru, G.; Ungureanu, R.; Banici, R.; Serbanescu, M.; Dabu, R.; Mourou, G.; Khazanov, E.A. 100 J-level pulse compression for peak power enhancement. *Quantum Electron.* **2017**, *47*, 173–178. [CrossRef]

27. Fisher, R.A.; Kelley, P.L.; Gustafson, T.K. Subpicosecond Pulse Generation Using The Optical Kerr Effect. *Appl. Phys. Lett.* **1969**, *14*, 140–143. [CrossRef]

28. Mourou, G.; Cheriaux, G.; Radier, C. Device for Generating a Short Duration Laser Pulse. U.S. Patent Application US20110299152A1, 8 December 2011.

29. Mourou, G.; Mironov, S.; Khazanov, E.; Sergeev, A. Single cycle thin film compressor opening the door to Zeptosecond-Exawatt physics. *Eur. Phys. J. Spec. Top.* **2014**, *223*, 1181–1188. [CrossRef]

30. Khazanov, E.; Mironov, S.Y.; Mourou, G. Nonlinear compression of high-power laser pulses: Compression after compressor approach. *Uspekhi Fiz. Nauk* **2019**, *189*, 1173–1200. [CrossRef]

31. Mironov, S.Y.; Ginzburg, V.N.; Lozhkarev, V.V.; Luchinin, G.A.; Kirsanov, A.V.; Yakovlev, I.V.; Khazanov, E.A.; Shaykin, A.A. Highly efficient second-harmonic generation of intense femtosecond pulses with a significant effect of cubic nonlinearity. *Quantum Electron.* **2011**, *41*, 963–967. [CrossRef]

32. Voronin, A.A.; Zheltikov, A.M.; Ditmire, T.; Rus, B.; Korn, G. Subexawatt few-cycle lightwave generation via multipetawatt pulse compression. *Opt. Commun.* **2013**, *291*, 299–303. [CrossRef]

33. Mironov, S.; Lassonde, P.; Kieffer, J.C.; Khazanov, E.; Mourou, G. Spatially-uniform temporal recompression of intense femtosecond optical pulses. *Eur. Phys. J. Spec. Top.* **2014**, *223*, 1175–1180. [CrossRef]

34. Mironov, S.Y.; Ginzburg, V.N.; Yakovlev, I.V.; Kochetkov, A.A.; Shaykin, A.A.; Khazanov, E.A.; Mourou, G.A. Using self-phase modulation for temporal compression of intense femtosecond laser pulses. *Quantum Electron.* **2017**, *47*, 614–619. [CrossRef]

35. Bleotu, P.G.; Wheeler, J.; Papadopoulos, D.; Chabanis, M.; Prudent, J.; Frotin, M.; Martin, L.; Lebas, N.; Freneaux, A.; Beluze, A.; et al. Spectral broadening for multi-Joule pulse compression in the APOLLON Long Focal Area facility. *High Power Laser Sci. Eng.* **2022**, *10*, E9. [CrossRef]

36. Mironov, S.Y.; Fourmaux, S.; Lassonde, P.; Ginzburg, V.N.; Payeur, S.; Kieffer, J.C.; Khazanov, E.A.; Mourou, G. Thin plate compression of a sub-petawatt Ti:Sa laser pulses. *Appl. Phys. Lett.* **2020**, *116*, 241101. [CrossRef]

37. Ginzburg, V.; Yakovlev, I.; Zuev, A.; Korobeynikova, A.; Kochetkov, A.; Kuzmin, A.; Mironov, S.; Shaykin, A.; Shaikin, I.; Khazanov, E.; et al. Fivefold compression of 250-TW laser pulses. *Phys. Rev. A* **2020**, *101*, 013829. [CrossRef]

38. Ginzburg, V.; Yakovlev, I.; Kochetkov, A.; Kuzmin, A.; Mironov, S.; Shaikin, I.; Shaykin, A.; Khazanov, E. 11 fs, 15 PW laser with nonlinear pulse compression. *Opt. Express* **2021**, *29*, 28297. [CrossRef] [PubMed]

39. Kim, J.I.; Kim, Y.G.; Yang, J.M.; Yoon, J.W.; Sung, J.H.; Lee, S.K.; Nam, C.H. Sub-10 fs pulse generation by post-compression for peak-power enhancement of a 100-TW Ti:Sapphire laser. *Opt. Express* **2022**, *30*, 8734. [CrossRef]

40. Available online: https://www.zeonex.com/displays-touch-sensors.aspx.html (accessed on 24 February 2017).

41. Laserix. Available online: http://hebergement.u-psud.fr/laserix/en/Laserix (accessed on 12 December 2019)

42. Lassonde, P.; Mironov, S.; Fourmaux, S.; Payeur, S.; Khazanov, E.; Sergeev, A.; Kieffer, J.C.; Mourou, G. High energy femtosecond pulse compression. *Laser Phys. Lett.* **2016**, *13*, 075401. [CrossRef]

43. Taylor, A.J.; Clement, T.S.; Rodriguez, G. Determination of n_2 by direct measurement of the optical phase. *Opt. Lett.* **1996**, *21*, 1812. [CrossRef]

44. Hult, J. A Fourth-Order Runge – Kutta in the Interaction Picture Method for Simulating Supercontinuum Generation in Optical Fibers. *J. Light. Technol.* **2007**. *25*, 3770–3775. [CrossRef]
45. Bespalov, V.; Talanov, V. Filamentary Structure of Light Beams in Nonlinear Liquids. *ZhETF Pisma* **1966**, *3*, 471–476.
46. Rubenchik, A.M.; Turitsyn, S.K.; Fedoruk, M.P. Modulation instability in high power laser amplifiers. *Opt. Express* **2010**, *18*, 1380–1388. [CrossRef] [PubMed]
47. Voronin, A.A.; Zheltikov, A.M. Pulse self-compression to single-cycle pulse widths a few decades above the self-focusing threshold. *Phys. Rev. A* **2016**, *94*, 023824. [CrossRef]
48. Mironov, S.Y.; Wheeler, J.A.; Khazanov, E.A.; Mourou, G.A. Compression of high-power laser pulses using only multiple ultrathin plane plates. *Opt. Lett.* **2021**, *46*, 4570. [CrossRef] [PubMed]
49. Li, Z.; Kato, Y.; Kawanaka, J. Simulating an ultra-broadband concept for Exawatt-class lasers. *Sci. Rep.* **2021**, *11*, 151. [CrossRef] [PubMed]